Groundwater

Hydraulic Conductivity Calibration of Logging NMR in a Granite Aquifer, Laramie Range, Wyoming

by Shuangpo Ren[1,2], Andrew D. Parsekian[2], Ye Zhang[2], and Bradley J. Carr[2]

Abstract

In granite aquifers, fractures can provide both storage volume and conduits for groundwater. Characterization of fracture hydraulic conductivity (K) in such aquifers is important for predicting flow rate and calibrating models. Nuclear magnetic resonance (NMR) well logging is a method to quickly obtain near-borehole hydraulic conductivity (i.e., K_{NMR}) at high-vertical resolution. On the other hand, FLUTe flexible liner technology can produce a K profile at comparable resolution but requires a fluid driving force between borehole and formation. For three boreholes completed in a fractured granite, we jointly interpreted logging NMR data and FLUTe K estimates to calibrate an empirical equation for translating borehole NMR data to K estimates. For over 90% of the depth intervals investigated from these boreholes, the estimated K_{NMR} are within one order of magnitude of K_{FLUTe}. The empirical parameters obtained from calibrating the NMR data suggest that "intermediate diffusion" and/or "slow diffusion" during the NMR relaxation time may occur in the flowing fractures when hydraulic aperture are sufficiently large. For each borehole, "intermediate diffusion" dominates the relaxation time, therefore assuming "fast diffusion" in the interpretation of NMR data from fractured rock may lead to inaccurate K_{NMR} estimates. We also compare calibrations using inexpensive slug tests that suggest reliable K_{NMR} estimates for fractured rock may be achieved using limited calibration against borehole hydraulic measurements.

Introduction

Hydraulic conductivity (K) is one of the most important properties for the evaluation, management, and remediation of groundwater resources. There are numerous direct and indirect methods that can be used, alone or in combination, to obtain K estimates for porous and fractured aquifers. Direct hydraulic measurements, such as a pumping test can give average K estimates over an entire producing zone of the aquifer (e.g., several tens of meters). However, when vertical heterogeneity needs to be quantified, such methods often prove insufficient. As an alternative, hydraulic methods that can characterize K at different vertical resolution have been developed, including multilevel slug tests, borehole flowmeter logging, dipole-flow tests, direct push permeameter (DPP), and FLUTe liner profiling (Zlotnik and McGuire 1998; Zlotnik et al. 2001; Butler et al. 2007; Paradis et al. 2011; Keller et al. 2014). Although such methods can provide information about hydraulic conductivity distribution of the investigated intervals, some limitations exist. For example, the DPP method has a maximum depth of investigation that is limited by the ability to advance a direct-push probe (e.g., Butler et al. 2007). The accuracy of multilevel slug test can be highly sensitive to the construction and development of the well and the potential existence of fluid leakage pathways among the packer assemblage (e.g., Butler 2005). In low K aquifers, a potential problem with the impeller flowmeter is that it must be trolled at sufficiently high speeds in order to run above the stall velocity of the flowmeter. However, when the trolling velocity is too high, the slow borehole flows cannot be accurately determined. For low-flow rates, Molz et al. (1989) recommended a heat-pulse flowmeter. The FLUTe liner uses a driving head inside the liner to displace water in the borehole into the formation as the liner descends and fills the well (Keller et al. 2014). Also, the detection limit of liner profiling is a function of the descent velocity of the liner as it is deployed into the well, and when the descent velocity of the liner is relatively large, small groundwater velocity changes can be missed, so that the FLUTe profiling transmissivity can

[1]Corresponding author: Key Laboratory of Tectonics and Petroleum Resources of Ministry of Education, China University of Geosciences, No. 388 Lumo Road, Wuhan 430074, China; cugspren@hotmail.com

[2]Department of Geology and Geophysics, University of Wyoming, 1000 E. University Ave, Laramie, WY.

Article Impact Statement: A joint interpretation of logging NMR data and FLUTe K estimates are used to calibrate the SDR equation in a fractured granite aquifer.

Received November 2017, accepted May 2018.

doi: 10.1111/gwat.12798

be less accurate and precise than the short interval straddle packer tests (Quinn et al. 2015, 2016). Short interval straddle packer tests are also more accurate and precise than the flowmeter logging methods. However, packer tests can be much more time consuming and expensive than both flowmeter logging and FLUTe profiling.

Borehole and surface geophysical surveys are the primary means of providing indirect measurements of aquifer properties (Rubin and Hubbard 2005). Compared to the direct measurements, geophysical methods have the advantage of being deployed rapidly and without employing fluid-flow-driving forces. However, the majority of the geophysical methods do not directly estimate K values and therefore, transform functions are needed to translate geophysical properties to hydrogeologic properties. The logging nuclear magnetic resonance (NMR) method has been widely used in the petroleum industry for measuring lithology-independent porosity, fluid typing, and pore system analysis since the late 1980s (e.g., Coates et al. 1991a; Kenyon et al. 1995; Alvarado et al. 2003). A variety of studies have also reported its application to estimate intrinsic permeability (k) of many kinds of petroleum reservoirs, for instance, consolidated sandstone (Kenyon et al. 1988; Straley et al. 1997; Kleinberg et al. 2003), carbonates (Chang et al. 1994; Kenyon et al. 1995; Allen et al. 2000; Alvarado et al. 2003), and shale (Prammer 1994). Thanks to the recent development of a small diameter NMR logging tool specifically designed for near-surface applications (Walsh et al. 2013), logging NMR has been extended to infer near-wellbore K in unconsolidated aquifers (e.g., Dlubac et al. 2013; Knight et al. 2016). NMR-derived parameters obtained from logging are typically expected to require calibration against direct K estimates through a transform model to enable accurate K predictions. Presently, an equation developed by Schlumberger Doll Research (SDR) is the most commonly used transform model to obtain estimates of formation flow properties from NMR parameters (Kenyon et al. 1988; Coates et al. 1991b). A set of standard empirical constants have been determined through numerous laboratory studies and have been proved effective for estimating permeability for consolidated materials and rocks (Coates et al. 1999; Dunn et al. 2002; Ellis and Singer 2007). For unconsolidated materials, however, Hodgkins and Howard (1999) found that the application of the standard empirical SDR constants resulted in k_{NMR} estimates that were biased by several orders of magnitude from true formation permeabilities. Dlubac et al. (2013) optimized the fit between an upscaled NMR-derived K and a wellbore flow (WBF) logging-derived K ($K_{\mathrm{WBF\text{-}logging}}$) to determine a set of site-specific empirical constants specifically for unconsolidated aquifer materials. For a diverse group of unconsolidated aquifers, Knight et al. (2016) compared the logging NMR and direct-push K data to acquire a set of optimized SDR constants for each site. They found little variability among the sets of the SDR constants from all sites, which suggests the possible existence of generalized SDR constants for determining K of near-surface unconsolidated aquifers.

It has been assumed that NMR cannot be calibrated to estimate flow properties in fractured aquifers because the surface area of the fractures estimated by NMR does not exert enough control on K (e.g., Dlugosch et al. 2013). However, Nakashima and Kikuchi (2007) and Xiao and Li (2011) have experimentally and numerically explored the sensitivity of NMR to fracture aperture, and therefore we are motivated to pursue testing of NMR for fractured rock flow properties.

In contrast to porous aquifers, the use of NMR logging to estimate K for fractured bedrock aquifers is limited. Most research into fracture characterization with the NMR technology focuses on determining fracture geometries and, depending on the implementation detail, can be divided into NMR spectroscopy, NMR imaging, and NMR relaxation-tomography (Chen et al. 1995; Chang et al. 1997; Kumar et al. 1997; Borgia et al. 1999; Golsanami et al. 2016). Nakashima and Kikuchi (2007) proposed a method for estimating fracture apertures using NMR logging, a first quantitative evaluation of fractures of this kind. In that study, they established a lithology independent linear relationship between free fluid porosity (i.e., porosity of fractures whose aperture is greater than 0.2 mm) and fracture aperture by calibrating a NMR sensor on laboratory core samples. In natural bedrock aquifers, fracture dip can affect the raw NMR logging data and thereby affect the aperture calculation. In such environments, borehole image logging (e.g., electrical microimaging and borehole televiewer) was also necessary to identify the dip angle of the fractures. Xiao and Li (2011) used numerical simulation to systematically analyze the impact of fracture parameters, such as fracture width, density, and dip angles, on the NMR transverse relaxation time (i.e., T_2 distribution). Their results indicate that the existence of fractures affects NMR logging and its interpretation, while echo spacing, type of drilling fluids, and length of antennas also are thought to have an impact on the T_2 distribution. Xiao and Li (2011) modeled the NMR response to saturated fractures through bench scale laboratory experiments, but fracture hydraulic conductivity was not estimated.

In this study, we investigated the applicability of NMR logging to provide reliable estimates of hydraulic conductivity for a fractured granite aquifer. Based on K_{NMR} and K_{FLUTe} data obtained from three bedrock wells located in the Blair Wallis Fractured Rock Hydrology Research Well Field (BW-RWF) located in a mountain headwater watershed, near Laramie, Wyoming, we explore transform functions to predict K assuming parallel fractures to obtain a set of well-specific NMR parameters. By comparing these parameters among the three boreholes, we investigate whether a set of "universal" constants can be identified for this fractured aquifer.

Background

NMR Background

In the presence of an external static magnetic field B_0, produced by a strong permanent magnet within the NMR

tool, the hydrogen nucleus will be subjected to magnetic induction until reaching a new equilibrium state, and in the meanwhile, a small net nuclear magnetization is generated in the direction parallel to B_0 (Dunn et al. 2002). An external oscillating excitation field B_1 is generated using an internal coil, tipping the magnetization into the plane perpendicular to the background static magnetic field B_0. The initial amplitude of the relaxation signal at the beginning of the measurement is related to the volume of water present within the bulk volume being measured. The relaxation time associated with the decay of the magnetization in the transverse plane (perpendicular to B_0) is called T_2. Please refer to Behroozmand et al. (2015) for a thorough review of NMR principles related to near surface material characterization.

The transverse relaxation time, T_2, is sensitive to the geometry of water-filled pore space and can be considered as a proxy for a volume-averaged surface-area-to-volume-ratio (Brownstein and Tarr 1979). Generally, water in small pores relaxes more quickly than that in larger pores (Kleinberg and Griffin 2005). For water in pores that are fully saturated, T_2 is determined by combining three well-known relaxation mechanisms for the NMR measurements:

$$T_2^{-1} = T_{2\text{bulk}}^{-1} + T_{2\text{surface}}^{-1} + T_{2\text{diffusion}}^{-1} \tag{1}$$

where $T_{2\text{bulk}}$ is bulk relaxation time, $T_{2\text{surface}}$ is surface relaxation time, and $T_{2\text{diffusion}}$ is diffusion-induced relaxation time due to the presence of inhomogeneities in the background magnetic field. In NMR physics, diffusion refers to the movement of water molecules throughout their pore environment, rather than chemical solute transport. As water molecules and the associated excited proton (H^+) move within the pores space over the timescale of an NMR measurement, the excited H^+ will relax at different rates if B_0 is heterogeneous (e.g., due to the existence of paramagnetic sites on mineral grain surfaces). Alternatively, if B_0 is homogeneous and the pores are sufficiently small, the relaxation rate will be primarily controlled by the interactions of excited spins with pore walls.

For water relaxing in a single pore, Brownstein and Tarr (1979) defined three diffusion regimes based on the control parameter $\rho a/D$, where ρ is transverse surface relaxivity, a is the mean distance that a proton travels before encountering a paramagnetic site, and D is diffusion coefficient of bulk water. The fast diffusion regime, where $\rho a/D \ll 1$, all spins can travel to and relax at the pore surface in the time an NMR measurement is made, and a single pore contributes only a single relaxation time. The slow diffusion regime, where $\rho a/D \gg 10$, a spin does not sample the entire pore space before relaxing at the pore surface, and each pore size contributes several relaxation times to the overall signal. In the intermediate diffusion regime, where $1 < \rho a/D < 10$, again, a single pore contributes several relaxation times to the overall signal.

In the fast diffusion regime, Equation 1 can be simplified to:

$$\frac{1}{T_2} \approx \frac{1}{T_{2\text{surface}}} = \rho \left(\frac{\text{S}}{\text{V}}\right) \tag{2}$$

where S/V is ratio of pore surface to pore volume. On the other hand, in the slow diffusion regime, the NMR relaxation can be expressed as (Maurer and Knight 2016):

$$\frac{1}{T_2} \propto D \left(\frac{S}{V}\right)^2 \tag{3}$$

Thus, $\frac{1}{\text{T}_2} \propto \frac{\text{S}}{\text{V}}$ for the fast diffusion regime, while in slow diffusion, $\frac{1}{\text{T}_2} \propto \left(\frac{\text{S}}{\text{V}}\right)^2$. In addition, for the slow-diffusion regime, T_2 is no longer a function of ρ (e.g., Dlugosch et al. 2013; Maurer and Knight 2016), which reflects a reduced influence of pore-wall interactions during diffusion relaxation in the saturated environment.

Permeability Estimation from NMR Data

For the purpose of using NMR logging data to estimate permeability (k) or hydraulic conductivity (K), a reliable relationship between the NMR T_2 distribution and k (or K) is necessary. For porous materials, the Kozeny-Carman equation (Kozeny 1927; Carman 1937) relates k of a porous material to its total porosity Φ and S/V:

$$k = \beta \frac{\Phi}{\left(\frac{S}{V}\right)^2} \tag{4}$$

where β is a dimensionless constant that captures the tortuosity and pores geometry within the material (Gueguen and Palcaiuckas 1994). Based on Equation 4, the SDR equation for porous media is developed by replacing (S/V) of Equation 4 with the mean of the $\log(T_2)$ distribution, $T_{2\text{ML}}$, and by adding a set of empirical constants (Kenyon et al. 1988; Straley et al. 1997).

$$k = b\Phi^m \left(T_{2\text{ML}}\right)^n \tag{5}$$

where b, m, and n are determined empirically if k, Φ, and $T_{2\text{ML}}$ are independently measured. For consolidated materials, b, related to tortuosity and pore geometry, is frequently calibrated to be approximately at 4 mD ms^{-2} (Kenyon et al. 1988). The porosity exponent m is dimensionless and is associated with Archie's formation resistivity factor (Chang et al. 1994). The relaxation time exponent, n, is assumed to be related to grain size distribution with a reported range between 1.4 and 2 (Dunn et al. 1999). Under the fast diffusion assumption, n is typically held at 2 in order to conform to the dimensions of (S/V) in the Kozeny-Carman equation. However, if the relaxation occurs in slow diffusion, n should be held at 1 for $\frac{1}{\text{T}_2} \propto \left(\frac{\text{S}}{\text{V}}\right)^2$, and $k \propto T_2$. Maurer and Knight (2016) summarized the reported b, m, and n values from the literature. For consolidated materials, b varies by three orders of magnitude among geologic formations, while

$m = 4$ and $n = 2$ are the most commonly reported values. Because the NMR relaxation properties are, in part, a function of pore geometry and magnetic mineralization, the latter varies in both type and quantities in geologic formations, the above values suggest that for different geological formations, calibration of formation-specific SDR parameters is necessary to obtain k from NMR parameters.

For a rock with a set of parallel fractures, a transform relation similar to the SDR equation can be derived for a radial flow model between $N+1$ parallel disks (assuming the thickness of the model is 1 m). Assuming all fractures are identical and have the same aperture and flow only occurs in fractures, an equivalent conductivity K can be defined as:

$$K = \frac{\rho_w g N B^3}{12\mu} \tag{6}$$

where ρ_w is water density [M/L^3], g is gravitational acceleration constant [L/T^2], N is number of flowing fractures per unit distance normal to the fracture planes [1/L], B is fracture aperture [L], and μ is dynamic viscosity of water [M/LT]. An effective bulk fracture porosity Φ_f is:

$$\phi_f = BN \tag{7}$$

The S/V for a single fracture is:

$$\frac{S}{V} = \frac{2}{B} \tag{8}$$

The relationship between permeability (k) and hydraulic conductivity (K) is:

$$K = \frac{k\rho_w g}{\mu} \tag{9}$$

Combining Equations 6 through 9, the following relationship can be derived:

$$k = \frac{1}{3} \cdot \frac{\phi_f}{\left(\frac{S}{V}\right)^2} \tag{10}$$

Equation 10 for a conceptual fracture model has a similar form as Equation 4 for porous media. In investigating fractured granite, we assume that groundwater flow occurs only in the interconnected fractures because porosity of granite matrix is generally less than 1% and its permeability is on the order of 10^{-20} m^2 or less (Nakashima and Kikuchi 2007; Mohnke and Yaramanci 2008). Thus, NMR logging is expected to yield parameters related only to fractures. Furthermore, Equation 5, which modifies Equation 4 to account for non-ideal pore geometry and different mineralogy in porous media, is assumed applicable to determining k of fractured rocks from similar NMR parameters. Therefore, the SDR equation can be written for estimating hydraulic conductivity of fractured rock in the same form as porous media as:

$$K_{NMR} = b\ \Phi^m\ (T_{2ML})^n \tag{11}$$

where K_{NMR} is fractured rock conductivity estimated from the NMR data. Again, b is considered to be lithology-dependent and is assumed related to surface relaxivity ρ.

In this research, at three open boreholes completed in a fractured granite, high-resolution K profiles (K_{FLUTe}) were obtained using a FLUTe blank liner (Keller et al. 2014). In the same boreholes, NMR logging was also carried out to obtain bulk fracture porosity and T_{2ML} profiles. At a given well location, based on a non-parametric bootstrap approach (Efron 1979), random subsets of the collocated borehole $K_{FLUTe,}$ NMR-porosity, and T_{2ML} profiles were drawn from a standard uniform distribution in order to determine a set of empirical NMR parameters and their associated ranges for the well (Parsekian et al. 2015). Given these parameters and their ranges, K_{NMR} uncertainty can then be evaluated.

Study Site and Methods

Well Field

The Blair Wallis Fractured Rock Hydrology Research Well Field lies in the Laramie Range near Laramie, Wyoming. The Laramie Range consists of Precambrian rocks that form outcrops from the Colorado-Wyoming border to the Powder River basin in southeastern Wyoming (Johnson and Hills 1976). At Blair Wallis, fractured granite is overlain by approximately 10 to 18 m of saprolite (Flinchum 2017). This investigation uses NMR and FLUTe logging data from three bedrock wells (i.e., BW5, BW6, and BW7) that are completed in the Sherman Granite, a Precambrian aged granite that is mainly composed of microcline, plagioclase, quartz, hornblende, biotite, and ilmenite (Frost et al. 1999). The wells were drilled as open hole in the fractured granite using the water/air rotary methods, thus drilling mud is not present in the boreholes. BW5 was drilled to a depth of 39.02 m and was cased with 4-in. PVC to a depth of 18 m; BW6 was drilled to a depth of 60.76 m and was cased with 6-in. PVC to a depth of 17 m; BW7 was drilled to a depth of 72.83 m and was cased with 6-in. PVC to a depth of 17 m. BW5 was drilled using a wireline coring system with water, while BW6 and BW7 were drilled with air/water rotary hammer. All three boreholes were developed using the airlift method before any logging activity. Below the casing, the boreholes are open and are fully saturated based on water level monitoring data collected in the same period from these boreholes.

Borehole Televiewer, Ambient Flowmeter, and Magnetic Susceptibility Logging

Along the open hole at each well, QL40-ABI-2G Borehole Televiewer (i.e., optical and acoustic) and QL40-SFM Spinner Flowmeter (Mt. Sopris Instruments, Denver,

Colorado) logging were jointly interpreted to identify flowing fractures under ambient conditions (Ren et al. 2018).

The flowmeter logs were collected under ambient conditions in a trolling mode. In the Blair Wallis granite wells, the tool is operated under three distinct logging speeds (1.5, 3, and 6 m/min) both descending and ascending the borehole two distinct times (i.e., the tool was run up and down the hole 12 separate times). These extra runs up and down the borehole are analyzed for consistency after speed correction by a difference analysis. Each log is corrected for the speed of the tool traveling up or down the borehole based on tool calibrations run in a cased section of the borehole with known diameter. For the calibration runs in casing, it is assumed that within the cased section of the borehole that there is no (or much smaller than the resolution of the tool) ambient upflow or downflow. However, it should be noted that the stall spin of the tool will vary depending on the speed the flowmeter is moving up or down the hole relative to the in situ flow rate up or down the hole. Therefore, it would be very difficult to predict exactly what the zero count rate would be until trying to collect some data. Typically, spinner flowmeter data should be recorded at as slow a trolling rate as possible without actually stalling the impeller (i.e., recording zero counts in the raw data). In the granite boreholes of this study, the flowmeter logs were collected at 1.5 and 3.0 m/min. This is significantly faster than the estimated ambient flow rates determined by bucket tests during air-lifts. However, the diameter changes in these boreholes will affect the data. First of all, the flowmeter was always centralized in the hole, thus the impeller observed laminar flow which would have been less affected by slight changes in diameters that are less than 0.076 m (i.e. the exposed length of the impeller). Second, it is true that when boreholes change diameter consistently for more than 0.076 m the counts measured by the impeller will either go up slightly (in narrower boreholes) or go down slightly (in wider boreholes). For the boreholes profiled in this work, BW-5 was a core hole with no washouts and was only 4% narrower in the bottom 1/3 of the hole. BW-6 never showed any change in diameter greater than 3% throughout its length. BW-7 had one depth with a diameter change of 14%. It also contains two other fracture breakouts at 2.0 and 1.5 m in width, that is, 60 and 40% greater than borehole diameter, respectively. No observable changes were seen in the flowmeter response for BW5 and BW6. For BW7, the only detectable deviations were due to the two large fracture breakouts: the largest background shift was only 50 counts per second or approximately 12% deviation. Finally, if we were trying to use the ambient flowmeter data to calculate the actual flow rate, it would be possible to correct these two points in the curve. However, since we are simply identifying depths where the spinner flowmeter deviates from the trolling rate (up or down), a 12% adjustment to the recorded count rate still results in an observable change from the trolling rate. Moreover, we do find water coming in at distinct fractures and going up and/or down. For example, in the ambient state as shown in Figure 3g, BW5 produces water to hole from the bottom to 34 m. This water is moving up the borehole until approximately 29 and approximately 26 m where most of it is leaving the borehole. More water is produced to the hole just below the casing (~18 m) and approximately 23 m. This water is flowing down the hole and out the fractures at 26 m.

Borehole televiewer can be used to detect apparent fractures along the borehole well. However, small cracks are difficult to identify from the televiewer images, and also not all fractures identified are flowing fractures. Ambient flowmeter logging can be used to infer flowing fractures as well the locations of inflow and outflow from formation to borehole. Only the depth intervals that correspond to significant inflow and outflow zones (a cut-off value is used) are then considered as flowing fracture zones (see Ren et al. 2018 for details). Flowmeter logging can also be used to detect micro-open cracks that provide conduits for groundwater but cannot be identified by the televiewer. However, the number of microcracks cannot be easily determined by flowmeter logging alone, so we assume one equivalent aperture for the intervals that contain such tight but flowing cracks. An example is shown in Figure 3d. At approximately 29.1 m depth, we can see a significant outflow from flowmeter log, but the televiewer logs do not exhibit obvious fracture count at this depth. Thus, we attribute this to an equivalent flowing microcrack. This leads to more fractures in the flowing fracture density than in the televiewer fracture density at that depth. Please refer to Ren et al. (2018) for more details. We also measured a magnetic susceptibility log on each well using QL40-HM (Mt. Sopris, Denver, CO). These logs were acquired to (1) determine if the Sherman granite contained *Fe* and *Mg* that may impart magnetic gradients which can skew NMR results, and (2) to calculate transverse surface relaxivity (ρ) following Foley et al. (1996).

Hydraulic Conductivity Measured Using FLUTe Liner

FLUTe profiling is a high-resolution hydraulic method for estimating T along open boreholes (Keller et al. 2014). FLUTe profiling can be used to identify flowing fractures along the length of an open hole as well as their hydraulic conductivities. Compared to packer tests, FLUTe profiling can often be used to circumvent the leakage issues (Keller et al. 2014). It was used to profile K of the fractured bedrock of the three boreholes at Blair Wallis. Specifically, borehole K was measured using a blank FLUTe liner for the 21.02, 43.69, and 55.76 m intervals below the casings of BW5, BW6, and BW7, respectively.

The FLUTe blank liner was installed by filling the liner with water to create a hydraulic head differential between the inside and outside of the liner. This head differential causes the liner to descend down the hole. As the liner descends, it forces the water below the liner to flow out from the borehole and into the formation through flowing fractures. The descent rate of the liner at each depth is positively correlated with the transmissivity of

the remaining length of the open hole beneath the liner. With measurement of the change in velocity and the area of borehole cross section, a volumetric flow rate can be determined and transmissivity is obtained using the Thiem equation assuming steady state radial flow from borehole into the formation:

$$T = \frac{\Delta Q}{2\pi \Delta H} \ln\left(\frac{R}{r_w}\right) \quad (12)$$

where ΔQ [L^3/T] is the flow in the fracture that was sealed, T [L^2/T] is the transmissivity of a measured interval, ΔH [L] is the applied head difference, R [L] is an influence radius at which there is assumed to be no change in hydraulic head, and r_w [L] is the radius of the borehole. For this study, $\ln(R/r_w)$ is set to a value of ln(600), following Keller et al. 2014, and that the FLUTe estimated conductivity is largely insensitive to the approximate (but reasonable) range of this ratio. Equation 12 is used to obtain a T estimate for each increment of the borehole traveled in each time step. The flow rate is calculated for each change in the flow velocity as each fracture is sealed. The blank liner ultimately achieved a vertical resolution of approximate 0.3 m at the Blair well field. The many transmissivity data points can be summed over discrete intervals and the conductivity calculated by dividing the sum by the length of the interval summed. At each well, the liner was able to descend to approximately 70% of the open hole interval, with the bottom 30% not accessible due to the increasingly reduced transmissivity of the remaining open hole (i.e., an unreasonably long hydraulic equilibration time would be needed). The detection limit at our study site is approximately 10^{-10} m/s, which is assumed a lower bound of the hydraulic conductivity of the open hole. In this study, only reliable FLUTe K measurements are used. The permeable intervals identified by FLUTe profiling are mostly consistent with flowing fractured zones determined by borehole televiewer and flowmeter logging. For BW6, the permeable intervals identified from FLUTe profile are mostly consistent with flowing fracture zones, such as approximately 17 to 18, approximately 25 to 26, approximately 32, approximately 35 to 36, approximately 39 and approximately 43 m depth intervals. For low K zones, such as approximately 20 to 21, 23 to 25, approximately 38, and approximately 41 m, no flowing fractures are found at these depth intervals (Figure 1). Similar observations are also found for BW7. For BW5, FLUTe K profile does not show any extremely low K zones along the entire open hole, and correspondingly flowing fracture zones are also identified along the entire open hole.

Borehole NMR Measurements

The demodulated NMR relaxation data are fit with a multi-exponential function using software provided with the instrument to produce a T_2 relaxation time distribution (Walsh et al. 2013). Water content, or Φ when saturated, is calculated as the integral of the T_2 distribution, or the initial amplitude of the exponential relaxation function; both are mathematically equivalent. Downhole NMR data (i.e., porosity and T_2 distribution) were obtained for BW5, BW6 and BW7 with a Javelin JP350 (Vista Clara, Inc., Mukilteo, Washington) logging tool at 0.5 m intervals. Centralizers were not used within the borehole since there was only approximately 0.02 m available on each side of the tool—given this tight tolerance, we assume the tool is effectively centralized without an external apparatus. This tool was used to take measurements at four frequencies for each depth interval; each frequency corresponds to radial distance of investigation into the formation of 0.14, 0.16, 0.18, and 0.19 m from the center of the tool/borehole. Each radial distance of investigation corresponds to a shell several mm wide at the indicated radius because the distance between the tool and the measurement zone does not contribute to the signal. Each radial distance and frequency was collected using two recovery times (T_r) in order to maximize signal response from both long ($T_r = 4$ s, 12 stacks) and short relaxation ($T_r = 0.8$ s, 72 stacks) thereby allowing optimal measurement of both small (short) and large (long) pore environments. We then combined the T_2 relaxation time series from each of the four frequencies and used a moving-window averaging filter across the four radial depth intervals (~2 m) to increase the signal-to-noise ratio (SNR) and thus produced a set of final estimates of water content and relaxation time distribution. The mean log of the relaxation time distributions was calculated for use in developing the K transform relation based on Equation 11. All logging NMR data are available in the dataset Parsekian et al. (2017).

Data Analysis and Results

Hydraulic Conductivity Estimation

FLUTe profiling provided a vertical distribution of horizontal K at approximately 0.3 m intervals and horizontal K ranges over approximately three orders of magnitude from $1.0 \times 10^{-7.5}$ to $1.0 \times 10^{-4.5}$ m/s (Figure 1a). For all three boreholes, the FLUTe logs indicate a general trend of decreasing K with depth, while abrupt changes in K are also observed over short intervals such as in the 18 to 25 m depth zone (Figure 1a).

Slug tests were performed at the three boreholes to provide an alternative estimate of average horizontal K for each open interval. For each well, two slugs with different sizes were used (Ren et al. 2018). For a given slug size, at each well, slug-in and slug-out flow tests were performed twice (Ren et al. 2018). Using the Bouwer and Rice (1976) model for an unconfined aquifer, and consider potential well-skin and non-Darcian flow effects (both are determined to be negligible for BW5, BW6, and BW7, see Ren et al. 2018 for details), the average horizontal K calculated over the open hole interval is 3.02×10^{-6} to 3.13×10^{-6} m/s for BW5, 7.54×10^{-7} to 1.12×10^{-6} m/s for BW6, and 1.81×10^{-6} to 2.64×10^{-6} m/s for BW7. Moreover, the transmissivity

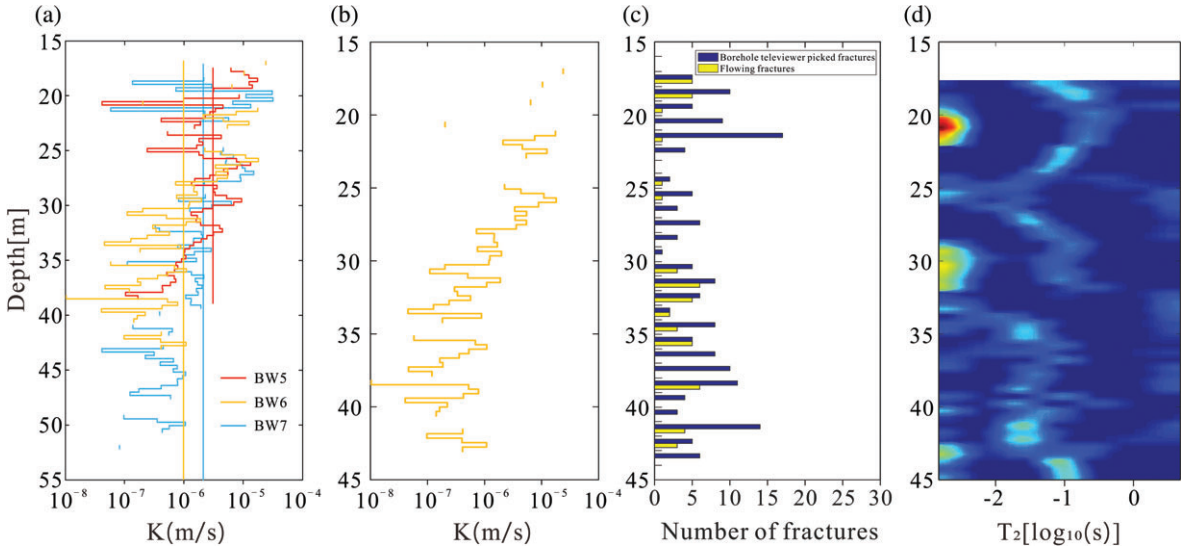

Figure 1. (a) FLUTe profiling every 0.3 m performed at three boreholes. An average horizontal K over the entire open borehole obtained from slug test is shown as a vertical solid line, color coded for the same wells. Note that only the intervals with reliable measurement are shown: K values below 10^{-10} m/s have been filtered out, (b) FLUTe profiling at BW6, (c) Fracture density picked from borehole televiewer and flowing fractures filtered by borehole flowmeter logging under ambient conditions for BW6, and (d) T_2 relaxation time distributions from BW6. Warm colors correspond to high frequency of water content.

values determined for the open hole using slug tests and FLUTe profiling are proved very close (Ren et al. 2018). The slug test results are also included in Figure 1a.

Fracture Density and NMR Signal Response to Flowing Fractures

For a depth interval from 18 to 28 bgs, Figure 2 presents fracture density determined from the televiewer logs and flowing fracture density determined from flowmeter logging. For either method, fracture densities were initially estimated at 0.25 m intervals and then upscaled to 1.0 m intervals. It is shown that fractures change laterally along the three test boreholes and only half of them are hydraulically active. Also, the borehole televiewer shows that low-angle fractures are dominant at the three test wells. Moreover, by applying the cubic law to the FLUTe transmissivity profile for each test interval and using the number of flowing fractures determined per test interval, an average hydraulic aperture for each test interval can be calculated. The calculated range of the average hydraulic aperture for BW5, BW6, and BW7 is 26 to 195 μm, 14 to 166 μm, and 33 to 200 μm, respectively (Ren et al. 2018). These calculated hydraulic apertures are comparable to reported literature, such as Quinn et al. (2011) calculated hydraulic apertures in a fractured dolostone aquifer.

The NMR T_2 distribution shows response to flowing fractures. Figure 3 showed a fracture zone in BW5 at 29.44 m that is identified by televiewer and caliper logs. The fracture is also open to flow, as confirmed by borehole flowmeter logging (Figure 3e). In Figure 3f, the NMR signal at nearly the same depth exhibits bimodal relaxation time distribution that indicates intrinsic pores and microcracks (i.e., at ~29.1 m), and fracture, respectively. It is also noteworthy that there are some zones

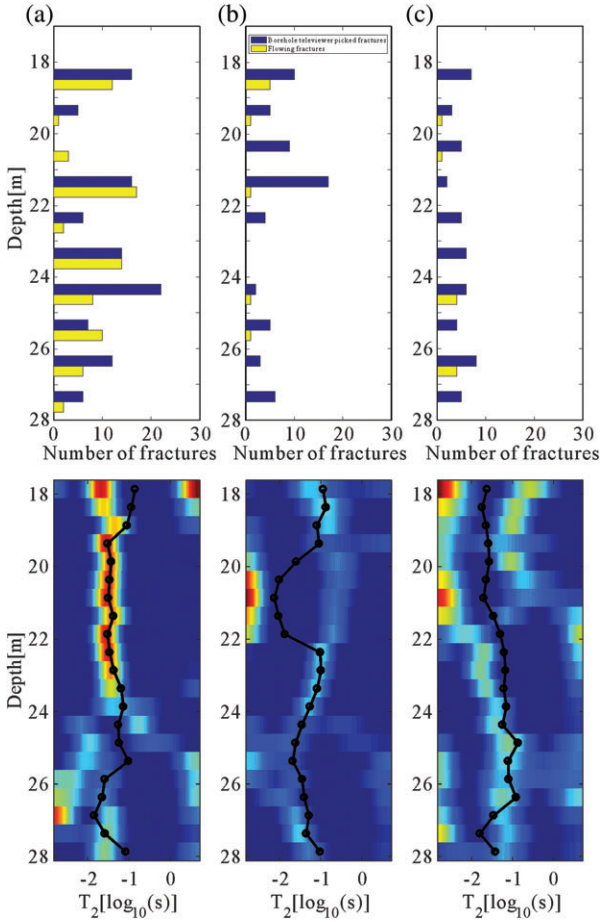

Figure 2. Fracture density, T_2 relaxation time distributions and the T_{2ML} values calculated from the distributions (circles connected by the solid line) for BW5 (a), BW6 (b), and BW7 (c) for depth interval from 18 to 28 m, respectively. Warm colors correspond to high frequency of water content.

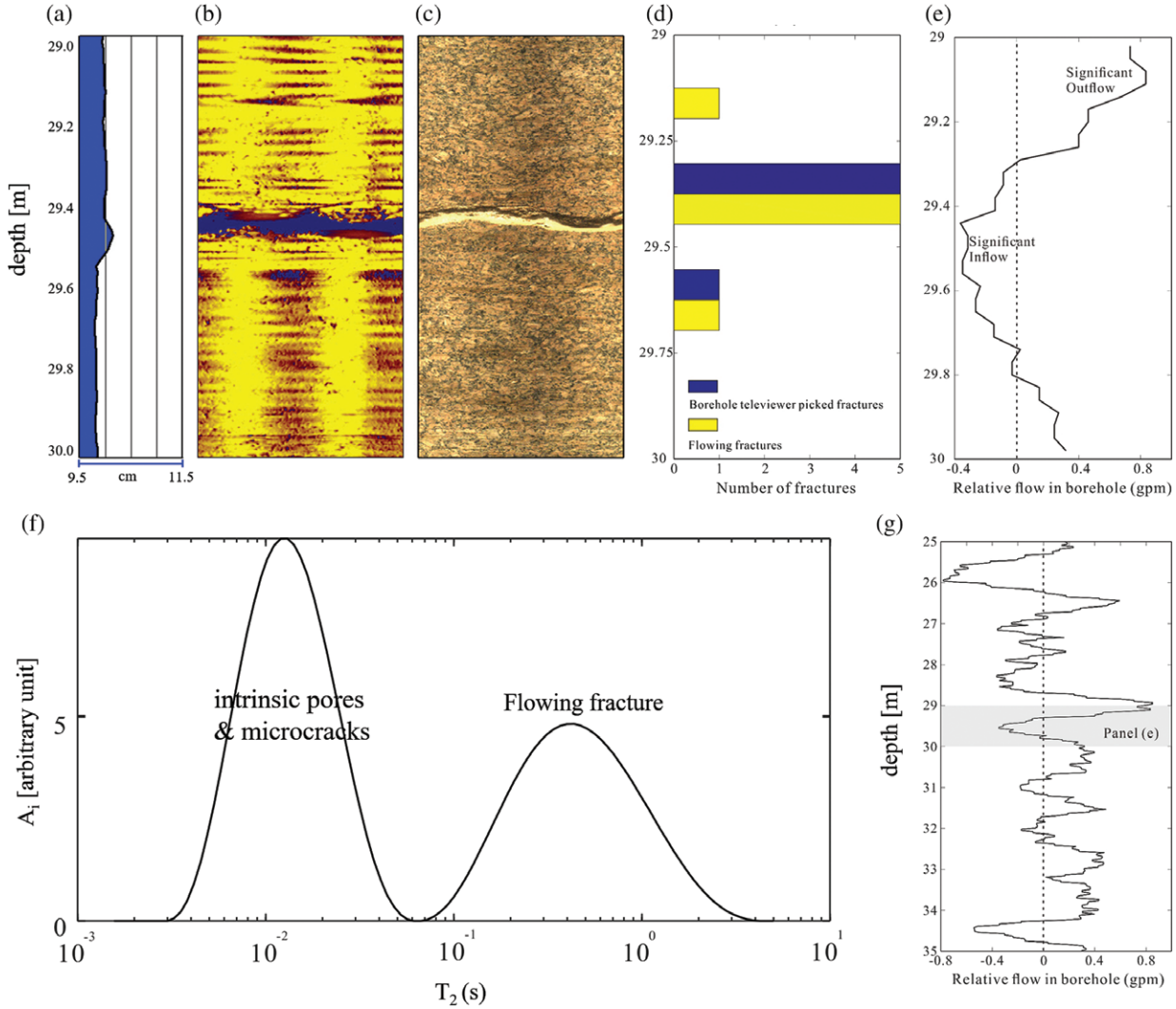

Figure 3. Borehole geophysical data in BW5 at the depth interval between 29 and 30 m bgs and corresponding flowmeter log, fracture counts, and T_2 distribution at the same depth. (a) Caliper log shows borehole diameter, (b) acoustic image log, (c) optical image log, (d) fracture counts, (e) flowmeter log, (f) T_2 distribution at nearly the same depth, and (g) flowmeter log between 25 and 35 m bgs at the same borehole.

where no flowing fractures are found but a large count in the non-flowing fractures are picked from borehole televiewer logs, which could be due to the existence of microcracks in granite, that is, intra and inter-granular fractures (Schild et al. 2001). Moreover, these zones could be due to the existence of filled fractures. However, as no thin-section study was carried out for the Blair Wallis wells, we cannot be certain of this. As an example, at approximately 20 to 22 m depth in BW6 (Figure 1c and d), we see a lot of televiewer picked fractures but very few flowing fractures. This could be due to the fact that this depth is close to the bottom of the saprolite which could provide fine sediments to fill these underlying fractures. Furthermore, we did not see much relationship between fracture counts and the distribution of water.

NMR Results and Estimation of NMR-Derived *K*

From about 10 to 18 m bgs to the bottom of each well, logging NMR data were collected along the fractured granite under fully saturated conditions. Figure 2 shows both the T_2 distributions and the calculated T_{2ML} of BW5, BW6 and BW7 that were inverted from the raw NMR signals using a nonlinear least squares method to invert the time series for the sum of exponentials where the exponent includes a $1/T_2$ term. Using the same approach for calculating SNR as Parsekian et al. (2013) used for surface NMR data (ratio of initial amplitude rms late-time noise), we find the SNR in our logging data range on average from 2.1 to 2.7. While this is somewhat low, this is expected due to the relatively low-total porosity in our fractured granite aquifer ($\sim$0.06 m^3 m^{-3}) in comparison with sediment porosity, and the typical noise level associated with logging NMR measurements of approximately 2%. For many depth intervals, the T_2 distributions are bimodal indicating both microcracks (or fracture-filling particulates, or intrinsic pores) and fractures. Based on collocated pairs of NMR and FLUTe data ($\pm$10 cm) from the three boreholes, we determined

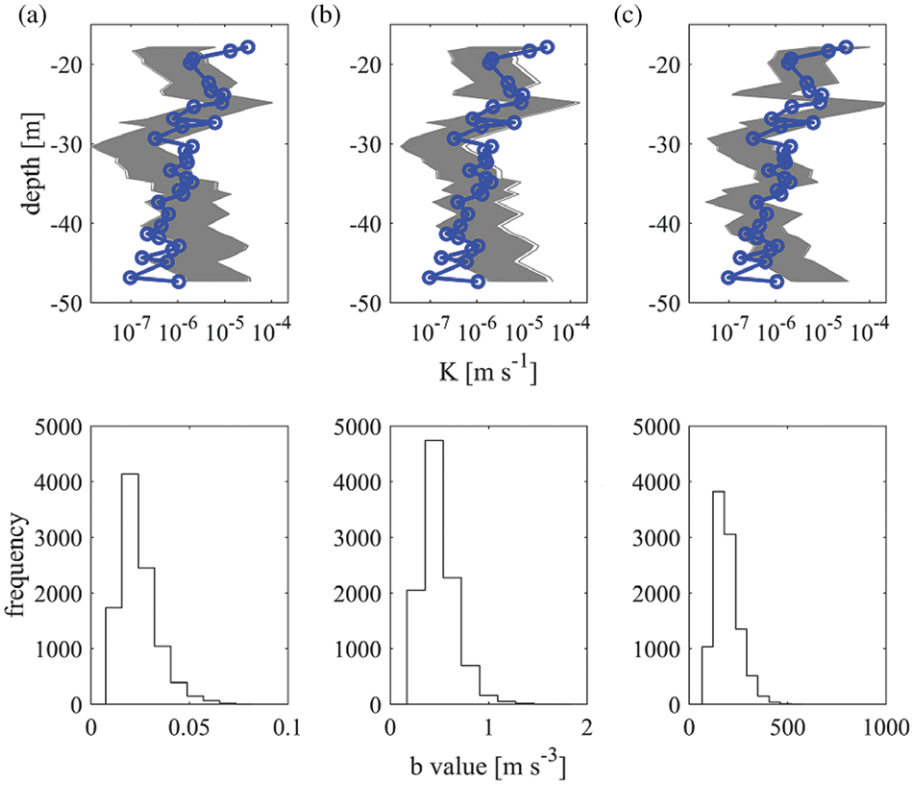

Figure 4. Example results from Well BW7 showing the effect of varying the m parameter while optimizing b using the bootstrapping method. (a) $m = 1$, (b) $m = 2$, (c) $m = 4$. Top panels show the FLUTe measured hydraulic conductivity (blue) and the results of the bootstrap simulations (gray) with three common used m values. Bottom panels show the distribution of SDR b parameter found through bootstrapping with different m values. Note that n is set to 2.

a set of optimal values for the empirical constants in Equation 11 using least-squares fitting, that is, minimizing the root mean square error (RMSE) between K_{NMR} and K_{FLUTe}. We first assigned $n = 2$ for the SDR equation, assuming that NMR relaxation occurs in the fast diffusion regime (Parsekian et al. 2015; Knight et al. 2016). We then determined the optimal values for the lithologic constant b using the commonly used values of 1, 2, and 4 for m. The results included distributions of optimized SDR b values and an estimation of K_{NMR} uncertainty around a mean value. The K_{NMR} uncertainty bound was calculated by bootstrapping (Parsekian et al. 2015): in this study, 50% of the total dataset and 10^4 re-samplings of the dataset were used. As a result, the normalized standard deviation of the SDR b parameter changed less than 10% and the threshold of least-squares residuals was normally distributed (Gong 1986).

At each borehole, substituting the Φ and $T_{2\mathrm{ML}}$ data derived from NMR relaxation distributions into Equation 11, a set of K_{NMR} profiles was obtained from 10^4 simulations using different values of $m = 1$, 2, and 4 (Figure 4). Note we only chose K_{FLUTe} values that were larger than the detection limit (10^{-10} m/s). Throughout our analysis we keep parameter $n = 2$ to honor the dimensions of S/V implied by the Kozeny-Carman equation. The bootstrapping results revealed that K_{NMR} estimated at each depth varies approximately 1 to 2 order of magnitude. Overall, K_{FLUTe} from well BW7 show a generally decreasing K with depth, while the optimized K_{NMR} ranges decrease until around 30 m before showing a slight tendency to increase. The variance in the optimized values given different porosity exponent, m, constants is relatively small, however generally using $m = 4$ supports sharper changes. Also shown in Figure 4 are the frequency distributions of the fitted b parameter to optimize each of the 10^4 bootstrap simulations. The resulting most frequent b values for each well and the associated standard deviations (σ) are in Table 1. The difference between most frequent b of the three boreholes became greater with increased m (i.e., when $m = 1$, difference between most frequent b are within a factor of 4; when $m = 2$, difference between most frequent b are within a factor of 6; when $m = 4$, difference between most frequent b are over a factor of 10). Figure 5 shows the estimated K for well BW7 with different m values when the entire K_{FLUTe} data set is used. For all the test intervals except the unsaturated zone, bottom of the well, and the depth around 30 m of the well, the estimate K is within one order of magnitude from K_{FLUTe}. The best fitted b parameters and RMSE between K_{NMR} and K_{FLUTe} are also given in Table 2.

For all three boreholes, the fit between the two conductivities is less accurate near the bottom of the hole. We attribute this to lower NMR signal as well as lower SNR at deeper depths. The NMR signal is positively proportional to saturated porosity, which is diminishing

Table 1

Most Frequent b Parameter Values Drawn from the Bootstrapping Simulation with Associated Standard Deviations and Root Mean Square Error

		b (m/s^{n+1})					
		$m = 1$		$m = 2$		$m = 4$	
n Value	Well Name	Most Frequent	σ	Most Frequent	σ	Most Frequent	σ
$n = 2$	BW5	3.41×10^{-2}	1.84×10^{-2}	1.17	6.90×10^{-1}	942.01	1113.90
	BW6	9.70×10^{-3}	1.71×10^{-2}	7.17×10^{-1}	5.11×10^{-1}	844.01	548.81
	BW7	1.12×10^{-2}	8.67×10^{-3}	1.94×10^{-1}	1.57×10^{-1}	81.78	63.82
$n = 1$	BW5	1.49×10^{-3}	5.29×10^{-4}	5.76×10^{-2}	2.17×10^{-2}	34.84	41.37
	BW6	5.68×10^{-4}	4.11×10^{-4}	2.47×10^{-2}	1.41×10^{-2}	13.95	17.24
	BW7	8.40×10^{-4}	2.54×10^{-4}	1.48×10^{-2}	4.52×10^{-3}	6.41	2.15

Note: Parameter values reported for various unitless m values.

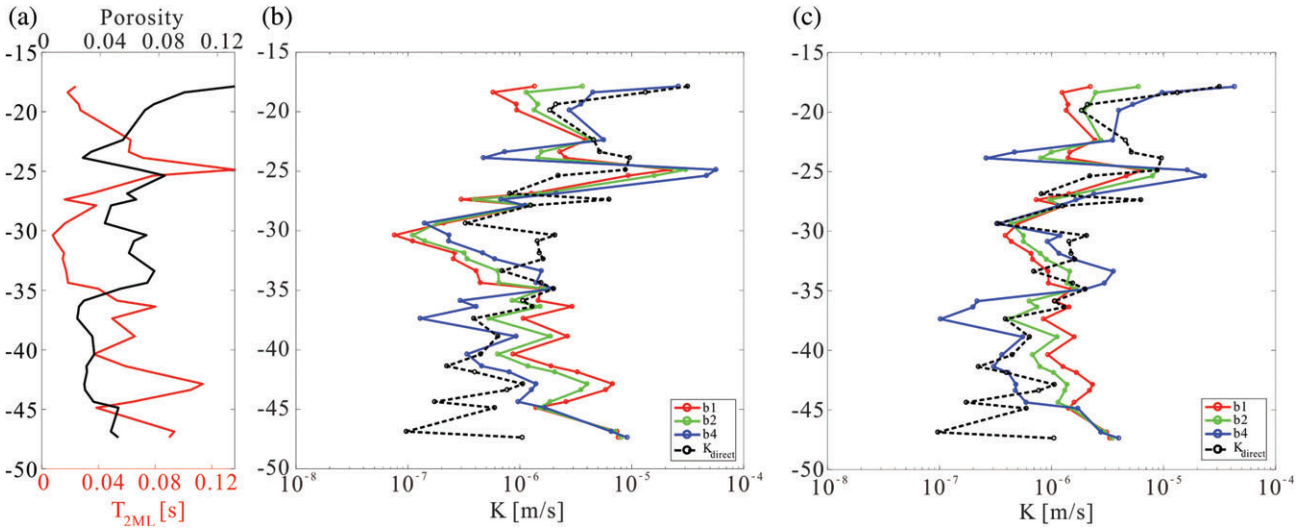

Figure 5. (a) Example from Well BW7 show the total porosity (solid black line) and the T_{2ML} values (solid red line) derived from NMR, (b) the estimated hydraulic conductivity using SDR equation (n is set to 2) with parameters from the porosity and the T_{2ML} values derived from NMR, and (c) the estimated hydraulic conductivity using SDR equation (n is set to 1) with parameters from the porosity and the T_{2ML} values derived from NMR. The optimized b value and corresponding m values are in Table 2. The open circles connected by the solid red line, solid green line and solid blue line indicate when $m = 1$, 2, and 4 are used, respectively. The open circles connected by the dashed black line (K_{direct}) indicate the FLUTe measured hydraulic conductivity.

Table 2

Optimized Value of b for Each Well Using Whole Data with Associated Root Mean Square Error

		$m = 1$		$m = 2$		$m = 4$	
n Value	Well Name	b (m/s^3)	RMSE (m/s)	b (m/s^3)	RMSE (m/s)	b (m/s^3)	RMSE (m/s)
$n = 2$	BW5	4.04×10^{-2}	1.09×10^{-5}	1.37	2.73×10^{-5}	1587.8	1.63×10^{-4}
	BW6	1.90×10^{-2}	2.09×10^{-6}	6.45×10^{-1}	2.59×10^{-6}	746.66	4.24×10^{-6}
	BW7	1.25×10^{-2}	6.77×10^{-5}	2.39×10^{-1}	2.08×10^{-4}	86.59	1.80×10^{-3}
$n = 1$	BW5	1.70×10^{-3}	1.80×10^{-6}	5.63×10^{-2}	3.52×10^{-6}	65.08	4.60×10^{-5}
	BW6	7.00×10^{-4}	7.47×10^{-6}	2.22×10^{-2}	7.39×10^{-6}	25.68	5.49×10^{-6}
	BW7	5.00×10^{-4}	2.59×10^{-6}	1.04×10^{-2}	1.43×10^{-5}	3.78	2.12×10^{-4}

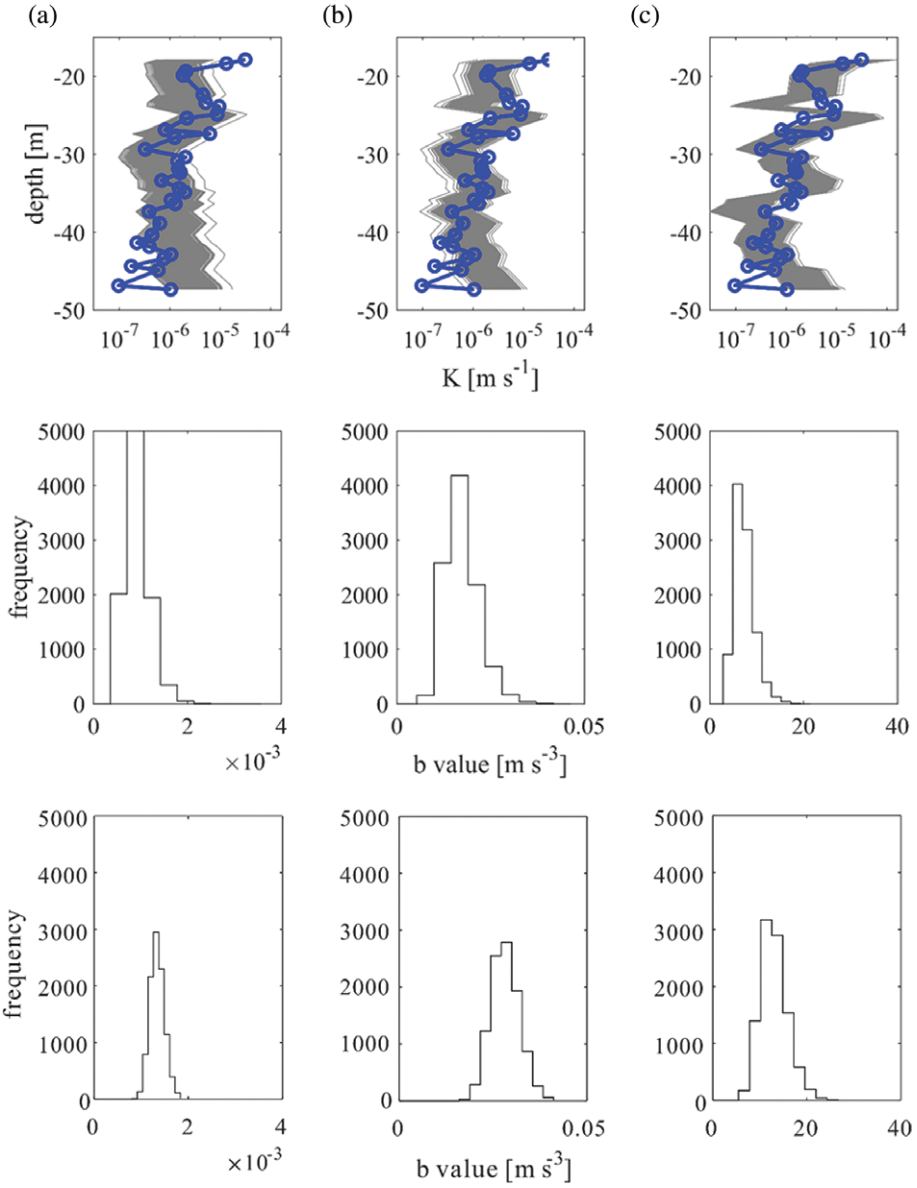

Figure 6. Example results from Well BW7 show the effect of varying the m parameter while optimizing b using the bootstrapping method. (a) $m = 1$, (b) $m = 2$, (c) $m = 4$. Top panels show the FLUTe measured hydraulic conductivity (blue) and the results of the bootstrap simulations (gray). Middle panels show the distribution of SDR b parameter found through bootstrapping with different m values. Bottom panels show the distribution of SDR b parameter found through bootstrapping calibrated with a single K value (shown in Figure 1a) from slug test. Note that n is set to 1.

with depth as can be seen from the K_{FLUTe} profiles and the number of identified flowing fractures.

Results of Varying *n*

Generally, the exponent n is typically set equal to 2 to be consistent with the exponent on S/V in the Kozeny-Carman equation under fast diffusion assumption. This is defensible for consolidated porous formations (Dunn et al. 1999). While in unconsolidated and fractured materials, as the pore size increases or when the fracture aperture is wide enough, this assumption may be violated and NMR relaxation would move into the slow diffusion regime (e.g., Dlugosch et al. 2013). However, at present there is not an independent indicator variable to determine the diffusion regime and when slow diffusion dominates, K should be proportional to T_2 decay. Therefore, we vary the n value (i.e., $n = 1$ and 2) to see which one can provide a more accurate K. Knight et al. (2016) also suggested that it is straightforward to calibrate the SDR equation with the exponent on the $T_{2\text{ML}}$ term (i.e., n) equal to 2 or 1 and evaluate the agreement between the estimated and measured values of K. Improved agreement with the exponent equal to 1 would suggest the presence of slow diffusion and this form of the SDR equation with corresponding b value could then be used to estimate K. Figure 6 shows the example results of BW7 from 10^4 bootstrapping simulations using the SDR equation with

$n = 1$, while m is set to 1, 2, and 4, respectively. The most frequent b values and the associated standard deviations (σ) are shown in Table 1. As m was increased, for all three boreholes, the difference between most frequent b values increased. However, a better fit was obtained when the whole dataset of a well was used, and the RMSE is always one order of magnitude smaller compared to $n = 2$ for different m values (Figure 5; Table 2).

Discussion

Impact of Different *m* Value on *K* Estimates

When n is fixed (1 or 2), the estimated K_{NMR} profiles are very similar with $m = 1$ or 2, although when m is set to 4, K_{NMR} shows greater fluctuation along the length of the well (Figures 4 and 6). Comparing our results to Parsekian et al. (2015) and Knight et al. (2016), when $m = 1$ or 2 is used: the most frequent b values are in the same order; however, when m is set to 4, our results are more than 2 orders of magnitude greater than theirs. This is due to the porosity of the fractured bedrock being very small at our field site (<10%, Figure 5a) compared to unconsolidated materials. Thus, the Φ^m component will become extremely small with increasing m, and the corresponding b values will increase simultaneously.

When the full data set from each well was used for calibration, the RMSE between K_{NMR} and K_{FLUTe} increased an order of magnitude as m was increased from 1 to 2, and then another order of magnitude when m was increased from 2 to 4 and therefore, $m = 1$ provided the best fit (Table 2). Figure 7 shows that ignoring porosity (see curve b0) can provide almost the same accuracy ($RMSE = 9.65 \times 10^{-6}$). We conclude that porosity does not improve the fit to the data, which is consistent with the findings of Maurer and Knight (2016).

Impact of Different *n* Values

Comparing the bootstrapping results for different n values, it is seen that the fluctuation range decreased by almost an order of magnitude with different m values when n is set to 1 (Figures 4 and 6). Furthermore, when the whole data set of each well was used for calibration, the fluctuation range of estimated K is also narrower by almost an order of magnitude when $n = 1$ is used (Figure 5), and the corresponding RMSE between estimated K and K_{FLUTe} also becomes an order of magnitude smaller (Table 2). To demonstrate $n = 1$ can better replicate the K_{FLUTe} measurements, a comparison using all data is shown in Figure 8, indicating that when $n = 1$ is used the values fall closer to the 1:1 line. These results show that the improved agreement between the estimated and measured values of K with $n = 1$, and suggest the dominance of slow diffusion in these fractures. However, even with $n = 1$, the difference between K_{NMR} and K_{FLUTe} is still greater than one order of magnitude at the top, bottom and a depth around 25 m of the well. We attribute this to (1) the increasing impact of T_{2bulk} in fractures with large aperture, which is neglected in the SDR equation (Dlugosch et al. 2013), and (2) the diffusion regime is very complicated in fractured rock. Actually, all the diffusion regimes (i.e., slow diffusion, intermediate diffusion and fast diffusion) are mainly dependent on fracture aperture, so one fixed parameter (i.e., $n = 1$ or 2) cannot satisfy all the situations. For the hydraulic aperture ranges from 14 to 200 μm at the three test wells, and the transition between fast diffusion and slow diffusion may occur frequently. The best fitting b values and the RMSE between estimated K and K_{FLUTe} with different n values are shown in Table 3, which can reflect the site-scale calibration to some extent. We see the RMSE between estimated K and K_{FLUTe} is one order of magnitude smaller when n is set to 1 compared to n is set to 2, indicating better estimated K when $n = 1$ is used. Moreover, in this study we only have approximately 4 orders of magnitude of K variability at this site so we cannot show how well the relationship holds at smaller or larger values. We anticipate that if we had more high K intervals, this relationship would be more visually log-linear. While the RMSE for $n = 2$ (Figure 8a) is high, when using a calibration where $n = 1$, we find the RMSE to be smaller, and many of the points fall within 1 order of magnitude. This is very similar to the result of Parsekian et al. (2015) or Allen et al. (2000). We should also point out that most of the outliers come from the bottom portions of the

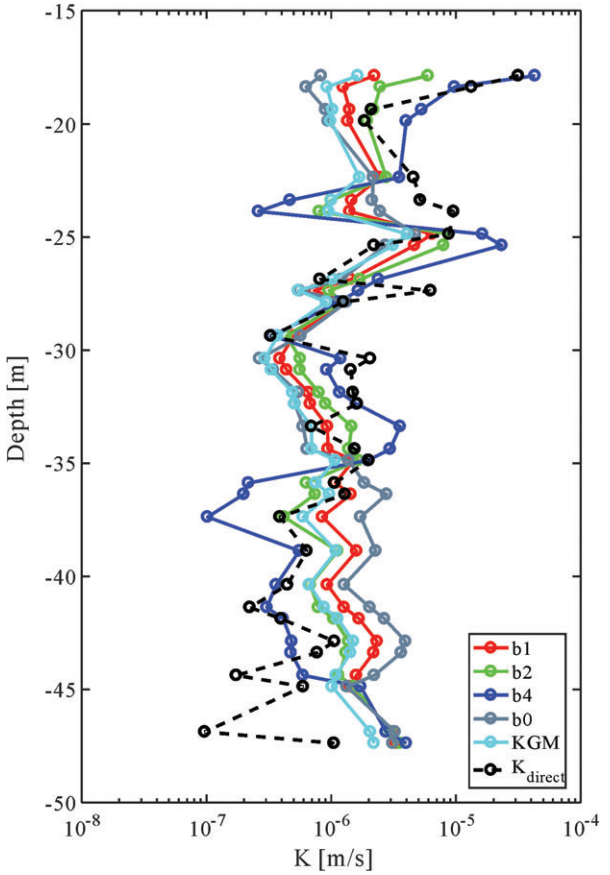

Figure 7. Example from Well BW7 show the estimated *K* using KGM compared with SDR equation with different m values. Note *n* is fixed to 1.

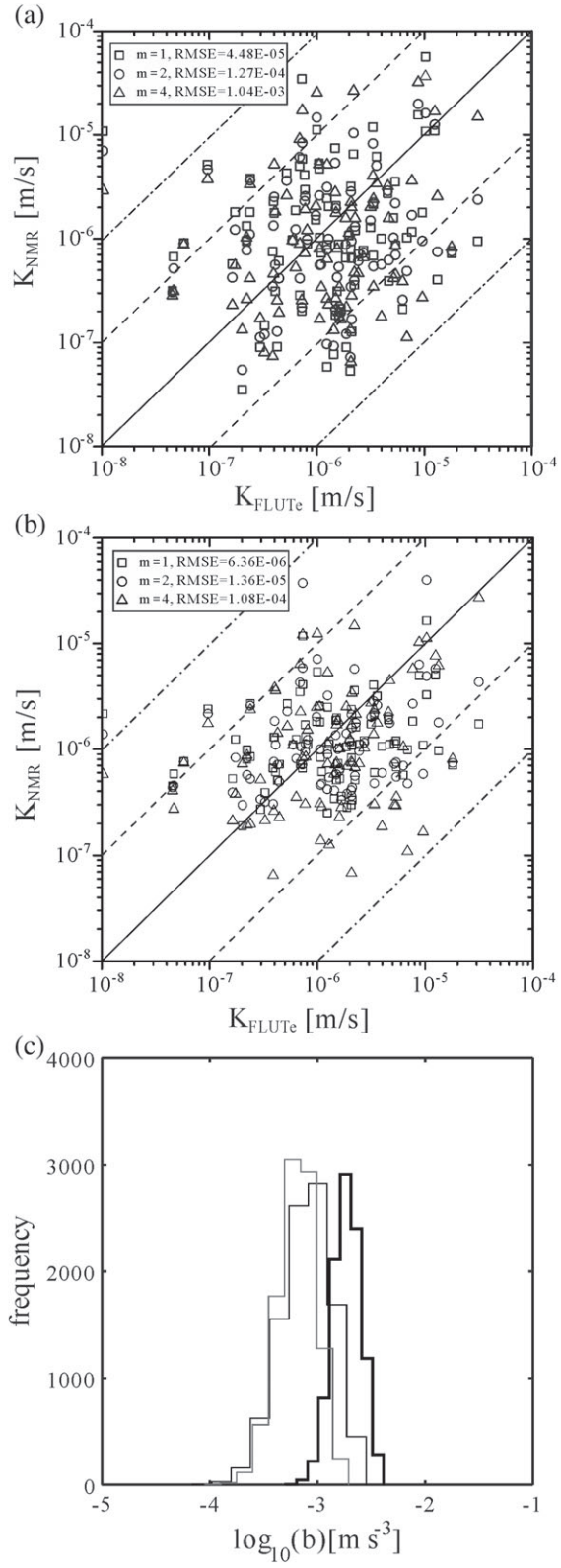

Figure 8. A 1:1 plot showing the correspondence between K_{FLUTe} values and K_{NMR} estimates using the whole dataset from all the three boreholes by changing the SDR equation with different empirical parameters. (a) $n = 2$, (b) $n = 1$. The dashed lines show an order of magnitude greater and less than the one-to-one line, and the dash dot lines show two order of magnitude greater and less than the one-to-one line. The distribution of b values for $n = 1$ at each well are shown in (c).

boreholes where the K is very low. We calculated the RMSE for the calibrated result using only the 20 to 40 m bgs data and found RMSE of 4.83×10^{-6}, 9.05×10^{-6}, and 8.79×10^{-5} for m = 1, 2, and 4.

Comparison of the SDR Empirical Constants within the Study Site

As shown in Table 1, for the bootstrapping simulations results, when $n = 2$ and $m = 1$ are used in the SDR equation, the most frequent b values for the three test wells range from 9.70×10^{-3} to 3.41×10^{-2} m/s^3, and the difference is within a factor of 4. While m is increased (i.e., m equal to 2, 4), both the most frequent b values and the differences between them increased. Furthermore, when m is equal to 4, the difference between most frequent b values is as large as two orders of magnitude. The same situation is also found when $n = 1$ (Table 1) and the whole data set of each well is used for calibration (Table 2). Knight et al. (2016) reported that it is feasible to define one b value for all unconsolidated materials. For fractured rock at Blair Wallis, our results showed that the best fitting b values for each well is not within a factor of 3 for the single Sherman Granite. This means that if calibration of the SDR equation parameters was performed at a one of the three boreholes and used to estimate K at another well, the resulting K would be more than a factor of 3 from the estimated K using the location-optimized b value. This is due to strong heterogeneity with widely varying hydraulic apertures at different locations at this site, which leads to different diffusion regimes. We interpret the factor of 3 difference observed here to be acceptable for doing a "local" calibration with one high-resolution K log that would be transportable to all wells at a wellfield. This is also demonstrated in Figure 8c where the b distributions ($m = 1$, $n = 1$) are plotted for each of the three wells calibrated to FLUTe K and substantial overlap is observed.

If high-vertical resolution K logs are unavailable, it would also be possible to achieve acceptable calibration using only a slug test in each well to obtain a bulk aquifer K value. To demonstrate this, we calibrated the NMR log at BW7 to a single K value from the slug test (using $n = 1$, Figure 6), and the most common values from the b distributions based on this bulk K calibration ($b = 1.23 \times 10^{-3}$, $m = 1$; $b = 2.48 \times 10^{-2}$, $m = 2$; $b = 10.15$, $m = 4$) are very similar to those resulting from the FLUTe K logs ($b = 8.40 \times 10^{-4}$, $m = 1$; $b = 1.48 \times 10^{-2}$, $m = 2$; $b = 6.41$, $m = 4$). This indicates that limited calibration against inexpensive bulk borehole hydraulic measurements would produce useful NMR K logs. This is a case for the Blair Wallis wells but its general applicability to other fractured rock sites remains to be tested.

Comparison of the SDR Empirical Constants between Fractured Granite and Other Types of Materials

For petroleum applications in consolidated materials, m is frequently fixed to 4, and n is fixed to 2, while for near-surface unconsolidated aquifer, n is always fixed to 2 but m is generally set to 1, 2, or 4. Knight

Table 3
Optimized Value of b Using Whole Data from Three Boreholes and Root Mean Square Error with Different n Value

	$m=1$		$m=2$		$m=4$	
	b (m/s^{n+1})	RMSE (m/s)	b (m/s^{n+1})	RMSE (m/s)	b (m/s^{n+1})	RMSE (m/s)
$n=2$	2.02×10^{-2}	4.48×10^{-5}	5.40×10^{-1}	1.27×10^{-4}	387.34	1.04×10^{-3}
$n=1$	8.00×10^{-4}	6.36×10^{-6}	2.16×10^{-2}	1.36×10^{-5}	15.50	1.08×10^{-4}

et al. (2016) compared a set of reported b values from consolidated sandstones, un/semi-consolidated material and unconsolidated material, and found that as one transition from unconsolidated to semi-consolidated and then to consolidated materials, the b value decreases by about an order of magnitude successively. In addition, for un/semi-consolidated materials, the optimal results for the empirical parameter m are found not always to be equal to 4. For example, Knight et al. (2016) found the optimal m is 1 and Dlubac et al. (2013) found the optimal m is 2. Compared with Parsekian et al. (2015) and Knight et al. (2016), when n is fixed to 2, our results (Table 1) indicate that the fitted b value is about two orders of magnitude greater than those b for unconsolidated sediments when m is set to 4, while when m is set to 1 or 2, fitted b is in the same order. If porosity is ignored (i.e., $m=0$) and n is fixed at 2, our best fitted b is 2 orders of magnitude smaller compared to Maurer and Knight (2016).

The Kozeny-Godefroy Model

For generalized pore geometry, Dlugosch et al. (2013) presented the Kozeny-Godefroy Model (KGM), an equation based on a combination of Kozeny-Carman and Godefroy et al. (2001) that may be optimized geometrically for planar, cylindrical, or spherical voids. Rather than depending on fitting parameters, the KGM model is physically based. It accounts for bulk water relaxation and is free from the diffusion regime assumption. Compared to the SDR equation, the KGM has the advantage of fewer empirical parameters without explicit physical definition, and all KGM parameters are known or can be obtained except tortuosity and surface relaxivity. For fractured granite, considering a planar geometry, the KGM is given by:

$$K = \frac{\rho_w g}{2\tau^2 \mu} \Phi \left(\frac{-D}{\rho} + \sqrt{\left(\frac{D}{\rho}\right)^2 + \frac{2DT_{2\text{bulk}}T_{2\text{ML}}}{T_{2\text{bulk}} - T_{2\text{ML}}}} \right) \tag{13}$$

where τ is the tortuosity [−]. $T_{2\text{bulk}}$, D, and ρ_w can be estimated as a function of temperature (Dlugosch et al. 2013), Φ and $T_{2\text{ML}}$ are from NMR measurement, g is always set to 9.81 m/s^2. For the boreholes of this work, we assumed the temperature θ is 6.5 °C from the long-term monitoring and calculated these temperature related parameters followed Dlugosch et al. (2013) (Table 1 in Dlugosch et al. 2013), while using the revised equation presented by Maurer and Knight (2016) to calculate diffusivity of water and the equation presented by Kestin et al. (1978) to calculate the viscosity of water (Equation 15 in Kestin et al. 1978). Results of these physical-based parameters are 2.0 for $T_{2\text{bulk}}$ (s), 1450.1 for μ (Pa s), 1.3×10^{-9} for D (m^2/s), and 999.95 for ρ_w (kg/m^3). We treat τ and ρ as fitting parameters, and then compared those with values from the literature.

Figure 7 shows an example of KGM estimated K compared with K estimated using the SDR equation ($n=1$) at BW7. Both equations provide the same accuracy in the estimated K: RMSE between K_{FLUTe} and the KGM estimated K is 1.20×10^{-5}, which is close to the value when $m=2$ is used in SDR equation (see Table 2). The best fitted τ and ρ are 1.38 and 8.52×10^{-5} m/s, respectively, which are consistent with reported values (e.g., Dlugosch et al. 2013). Dlugosch et al. (2013) speculate that the KGM will fail under the planar geometrical fracture case due to the lower influence of diffusion, however, in this study we demonstrate that this equation is also feasible for fractured rock, although the KGM model has more parameters whose estimation generally requires more measurements.

Quantitative Analysis of Diffusion Regime

Brownstein and Tarr (1979) used a control parameter $\rho a/D$ to divide diffusion regimes for water relaxing in a single pore. D is temperature dependent, which is calculated 1.3×10^{-9} m^2/s in this study. To calculate ρ, we followed Foley et al. (1996) using the magnetic susceptibility data of the fractured bedrock at the boreholes. We redefined a as the fracture hydraulic aperture for planar geometry which can be calculated using the Cubic Law:

$$B = \sqrt[3]{\frac{12\mu T}{\rho_w g N}} \tag{14}$$

where N is the number of flowing fractures in the same interval [−]. FLUTe can provide a T profile which can be used to estimate a distribution of B values along the open hole. For each well, $\rho a/D$ is computed along the depth of the borehole (Figure 9). $\rho a/D$ varies from −0.95 to 31.69, thus fast, intermediate, and slow diffusion all occurred at the tested wells (Brownstein and Tarr 1979). For all three boreholes, intermediate diffusion dominates (we attribute negative $\rho a/D$ to noise in the magnetic susceptibility

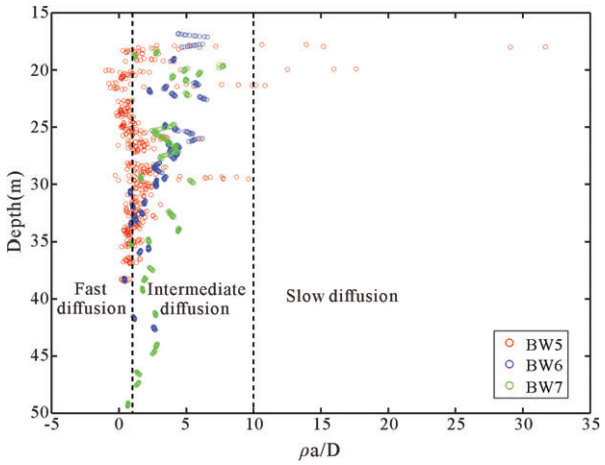

Figure 9. Calculated $\rho a/D$ along open hole for BW5, BW6, and BW7.

log and uncertainties in the estimated fracture aperture), which are in overall agreement with our observation that using an SDR parameter $n = 1$ indicating the presence of slow diffusion. However, not all aquifer intervals fall into the slow diffusion regime. The SDR n parameter is optimized across the entire borehole length and therefore aggregates the fast, intermediate, and slow diffusion occurring throughout the borehole.

Conclusions

In this study, we demonstrate the potential of using NMR logging measurements to provide estimates of hydraulic conductivity for a fractured granite aquifer. Overall, for over 90% of depth intervals the estimated K_{NMR} are within one order of magnitude of K_{FLUTe}. This agreement between K_{NMR} and direct conductivity measurements is similar to what has been observed in sedimentary aquifers. We found that, however, it is unrealistic to expect that one set of empirical parameter can be identified for a fractured aquifer. We also show that inexpensive slug test measurements may be used to adequately calibrate NMR data to estimate K along the length of the borehole. Although we found most values in this granite aquifer to be in the intermediate diffusion regime, for a fractured aquifer, it is quite possible that the relaxation occurs in the "slow-diffusion" regime when the aperture is sufficiently large. We observed a similar effect by changing the exponent on the $T_{2\mathrm{ML}}$ term—associated with sensitivity to the diffusion regime—from a value of 2 to 1 during the K calibration.

Acknowledgments

We thank the National Science Foundation for funding this research through EPSCoR Track I RII award #1208909 and MRI award #1531313. The financial support by International colleges and universities jointly cultivate doctoral program from China University of Geosciences (Wuhan) is greatly acknowledged. The authors would like to thank David Walsh, Carl Keller, Ty Ferre, and one anonymous reviewer for their insightful comments, which greatly improved this manuscript. We also acknowledge Nadia Fantello to attribute her work early on helping to set up the NMR/K conversion codes. All logging NMR data are available in the dataset Parsekian et al. (2017).

Authors' Note

The author(s) does not have any conflicts of interest or financial disclosures to report.

References

Allen, D., C. Flaum, T.S. Ramakrishnan, J. Bedford, K. Castelijns, C. Fairhurst, and R. Ramamoorthy. 2000. Trends in NMR logging. *Oilfield Review* 12, no. 3: 2–19.

Alvarado, R.J., A. Damgaard, P. Hansen, M. Raven, R. Heidler, R. Hoshun, J. Kovats, C. Morriss, D. Rose, and W. Wendt. 2003. Nuclear magnetic resonance logging while drilling. *Oilfield Review* 15, no. 2: 40–51.

Behroozmand, A.A., K. Keating, and E. Auken. 2015. A review of the principles and applications of the NMR technique for near-surface characterization. *Surveys in Geophysics* 36, no. 1: 27–85.

Borgia, G.C., V. Bortolotti, and P. Fantazzini. 1999. Magnetic resonance relaxation tomography to assess fractures induced in vugular carbonate cores. In *SPE Annual Technical Conference and Exhibition*. Houston, Texas: Society of Petroleum Engineers.

Bouwer, H., and R.C. Rice. 1976. A slug test for determining hydraulic conductivity of unconfined aquifers with completely or partially penetrating wells. *Water Resources Research* 12, no. 3: 423–428.

Brownstein, K.R., and C.E. Tarr. 1979. Importance of classical diffusion in NMR studies of water in biological cells. *Physical Review A* 19, no. 6: 2446–2453.

Butler, J.J. Jr., P. Dietrich, V. Wittig, and T. Christy. 2007. Characterizing hydraulic conductivity with the direct-push permeameter. *Groundwater* 45, no. 4: 409–419.

Butler, J.J. Jr. 2005. Hydrogeological methods for estimation of hydraulic conductivity. In *Hydrogeophysics*, ed. Y. Rubin, and S. Hubbard, 23–58. Dordrecht, the Netherlands: Springer.

Carman, P.C. 1937. Fluid flow through granular beds. *Transactions, Institute of Chemical Engineering* 15: 150.

Chang, D.H., J. Vinegar, C.E. Morriss, and C. Straley. 1994. Effective porosity, producible fluid and permeability in carbonates from NMR logging. In Transaction of the SPWLA Annual Logging Symposium. Society of Professional Well Logging Analysts. Paper A.

Chang, C.P., J. Qiao, S. Chen, and A.T. Watson. 1997. Fracture characterization with NMR spectroscopic techniques. *Journal of Magnetic Resonance* 126, no. 2: 213–220.

Chen, S., X. Yao, J. Qiao, and A.T. Watson. 1995. Characterization of fracture permeable porous media using relaxation-weighted imaging techniques. *Magnetic Resonance Imaging* 13, no. 4: 599–606.

Coates, G., M. Miller, M. Gillen, and G. Henderson. 1991a. An investigation of a new magnetic resonance imaging log. In *Transactions on SPWLA Annual Logging Symposium*. Paper DD.

Coates, G. R., T. C. A. Peveraro, A. Hardwick, and D. Roberts. 1991b. The magnetic resonance imaging log characterized by comparison with petrophysical properties and laboratory core data, paper SPE 22723. In *SPE Annual Technical*

Conference and Exhibition. Dallas, Texas: Society of Petroleum Engineers.
Coates, G.R., L. Xiao, and M.G. Prammer. 1999. *NMR Logging Principles and Applications*. Houston, Texas: Halliburton Energy Services.
Dlubac, K., R. Knight, Y. Song, N. Bachman, B. Grau, J. Cannia, and J. Williams. 2013. The use of NMR logging to obtain estimates of hydraulic conductivity in the high plains aquifer, Nebraska, USA. *Water Resources Research* 49: 1871–1886. https://doi.org/10.1002/wrcr.20151
Dlugosch, R., T. Günther, M. Müller-Petke, and U. Yaramanci. 2013. Improved prediction of hydraulic conductivity for coarse-grained, unconsolidated material from nuclear magnetic resonance. *Geophysics* 78, no. 4: EN55–EN64. https://doi.org/10.1190/geo2012-0187.1
Dunn, K.J., G.A. Latorraca, and D.J. Bergman. 1999. Permeability relation with other petrophysical parameters for periodic porous media. *Geophysics* 64, no. 2: 470–478.
Dunn, K.J., D.J. Bergman, and G.A. Latorraca. 2002. *Nuclear Magnetic Resonance: Petrophysical and Logging Applications*. Oxford, UK: Elsevier.
Efron, B. 1979. Bootstrap method: another look at the jackknife. *The Annals of Statistics* 7: 1–26.
Ellis, D.V., and J.M. Singer. 2007. *Well Logging for Earth Scientists*, 2nd ed., 691. Dordrecht, the Netherlands: Springer.
Flinchum, B. A. 2017. Imaging, characterizing, and understanding the critical zone: a near-surface geophysical perspective, Ph.D. dissertation, Department of Geology and Geophysics, University of Wyoming, Laramie, Wyoming, United States.
Foley, I., S.A. Farooqui, and R.L. Kleinberg. 1996. Effect of paramagnetic ions on NMR relaxation of fluids at solid surfaces. *Journal of Magnetic Resonance* 123: 95–104.
Frost, C.D., B.R. Frost, K.R. Chamberlain, and B.R. Edwards. 1999. Petrogenesis of the 1.43 Ga Sherman batholith, SE Wyoming, USA: A reduced, rapakivi-type anorogenic granite. *Journal of Petrology* 40, no. 12: 1771–1802. https://doi.org/10.1093/petroj/40.12.1771
Godefroy, S., J. Korb, M. Fleury, and R. Bryant. 2001. Surface nuclear magnetic relaxation and dynamics of water and oil in macroporous media. *Physical Review E* 64: 1–13.
Golsanami, N., J. Sun, and Z. Zhang. 2016. A review on the applications of the nuclear magnetic resonance (NMR) technology for investigating fractures. *Journal of Applied Geophysics* 133: 30–38.
Gong, S. 1986. Cross-validation, the jackknife, and the bootstrap: Excess error estimation in forward logistic regression. *Journal of the American Statistical Association* 81: 108–118.
Gueguen, Y., and V. Palcaiuckas. 1994. *Introduction to the Physics of Rocks*, 294. Princeton, New Jersey: Princeton University Press.
Hodgkins, M.A., and J.J. Howard. 1999. Application of NMR logging to reservoir characterization of low-resistivity sands in the Gulf of Mexico. *AAPG Bulletin* 83, no. 1: 114–127.
Johnson, R.C., and F.A. Hills. 1976. Precambrian geochronology and geology of the boxelder canyon area, northern Laramie range, Wyoming. *Geological Society of America Bulletin* 87, no. 5: 809–817.
Keller, C.E., J.A. Cherry, and B.L. Parker. 2014. New method for continuous transmissivity profiling in fractured Rock. *Groundwater* 52, no. 3: 352–367.
Kenyon, W.E., P.I. Day, C. Straley, and J.F. Willemsen. 1988. A three part study of NMR longitudinal relaxation properties of water saturated sandstones. *SPE Formation Evaluation* 3: 622–636.
Kenyon, W.E., R.L. Kleinberg, C. Straley, G. Gubelin, and C. Morriss. 1995. Nuclear magnetic resonance imaging—technology for the 21st century. *Oilfield Review* 7, no. 3: 19–33.
Kestin, J., M. Sokolov, and W.A. Wakeham. 1978. Viscosity of liquid water in the range −8°C to 150°C. *Journal of Physical and Chemical Reference Data* 7, no. 3: 941–948. https://doi.org/10.1063/1.555581
Kleinberg, R.L., and D.D. Griffin. 2005. NMR measurements of permafrost: unfrozen water assay, pore-scale distribution of ice, and hydraulic permeability of sediments. *Cold Regions Science and Technology* 42, no. 1: 63–77.
Kleinberg, R.L., C. Flaum, C. Straley, P.G. Brewer, G.E. Malby, E.T. Peltzer III., G. Friedrich, and J.P. Yesinowski. 2003. Seafloor nuclear magnetic resonance assay of methane hydrate in sediment and rock. *Journal of Geophysical Research* 108, no. B3: 2137. https://doi.org/10.1029/2001JB000919
Knight, R., D.O. Walsh, J.J. Butler, E. Grunewald, G. Liu, A.D. Parsekian, E.C. Reboulet, S. Knobbe, and M. Barrows. 2016. NMR logging to estimate hydraulic conductivity in unconsolidated aquifers. *Groundwater* 54, no. 1: 104–114.
Kozeny, J. 1927. Über kapillare Leitung des Wassers im Boden. Sitzungsberichte der Akademie der Wissenschaften in Wien Mathematisch- Naturwissenschaftliche Klasse, Abteilung IIa136, 271–306.
Kumar, A.A., P. Majors, W. Rossen, and U. Texas. 1997. Measurement of aperture and multiphase flow in fractures with NMR imaging. *SPE Formation Evaluation* 12, no. 2: 101–108.
Maurer, J., and R. Knight. 2016. Models and methods for predicting hydraulic conductivity in near-surface unconsolidated sediments using nuclear magnetic resonance. *Geophysics* 81, no. 5: D503–D518. https://doi.org/10.1190/GEO2015-0515.1
Mohnke, O., and U. Yaramanci. 2008. Pore size distributions and hydraulic conductivities of rocks derived from magnetic resonance sounding relaxation data using multi-exponential decay time inversion. *Journal of Applied Geophysics* 66, no. 3: 73–81.
Molz, F.J., R.H. Morin, A.E. Hess, J.G. Melville, and O. Guven. 1989. The impeller meter for measuring aquifer permeability variations—evaluation and comparison with other tests. *Water Resources Research* 25, no. 7: 1677–1683.
Nakashima, Y., and T. Kikuchi. 2007. Estimation of the apertures of water-saturated fractures by nuclear magnetic resonance well logging. *Geophysical Prospecting* 55, no. 2: 235–254.
Paradis, D., R. Lefebvre, R.H. Morin, and E. Gloaguen. 2011. Permeability profiles in granular aquifers using flowmeters in direct-push wells. *Groundwater* 49, no. 4: 534–547.
Parsekian, A.D., G. Grosse, J.O. Walbrecker, M. Müler-Petke, K. Keating, L. Liu, B.M. Jones, and R. Knight. 2013. Detecting unfrozen sediments below thermokarst lakes with surface nuclear magnetic resonance. *Geophysical Research Letters* 40: 1–6. https://doi.org/10.1002/grl.50137
Parsekian, A.D., K. Dlubac, E. Grunewald, J.J. Butler, R. Knight, and D.O. Walsh. 2015. Bootstrap calibration and uncertainty estimation of downhole NMR hydraulic conductivity estimates in an unconsolidated aquifer. *Groundwater* 53, no. 1: 111–122.
Parsekian, A.D., B.J. Carr, N. Claes, D.O. Walsh, and N. Fantello. 2017. *Borehole Nuclear Magnetic Resonance (NMR) Logging 2016-2017*. Laramie, Wyoming: University of Wyoming Research Data Repository.
Prammer, M.G. 1994. NMR pore size distributions and permeability at the well site. In *SPE Annual Technical Conference and Exhibition*. New Orleans, Louisiana.
Quinn, P.M., B.L. Parker, and J.A. Cherry. 2011. Using constant head step tests to determine hydraulic apertures in fractured rock. *Journal of Contaminant Hydrology* 126, no. 1–2: 85–99.
Quinn, P., J.A. Cherry, and B.L. Parker. 2015. Combined use of straddle packer testing and FLUTe profiling for hydraulic

testing in fractured rock boreholes. *Journal of Hydrology* 524: 439–454.

Quinn, P., B.L. Parker, and J.A. Cherry. 2016. Blended head analyses to reduce uncertainty in packer testing in fractured-rock boreholes. *Hydrogeology Journal* 24: 59–77. https://doi.org/10.1007/s10040-015-1326-2

Ren, S., S. Gragg, Y. Zhang, B.J. Carr, and G. Yao. 2018. Borehole characterization of hydraulic properties and groundwater flow in a crystalline fractured aquifer of a headwater mountain watershed, Laramie range, Wyoming. *Journal of Hydrology* 561: 780–795. https://doi.org/10.1016/j.jhydrol.2018.04.048

Rubin, Y., and S. Hubbard. 2005. *Hydrogeophysics, 523*, Vol. 50. Dordrecht, The Netherlands: Springer Water Science and Technology Library.

Schild, M., S. Siegesmund, A. Vollbrecht, and M. Mazurek. 2001. Characterization of granite matrix porosity and pore-space geometry by in situ and laboratory methods. *Geophysical Journal International* 146: 111–125.

Straley, C., D. Rossini, H.J. Vinegar, P. Tutunjian, and C.E. Morriss. 1997. Core analysis by low-field NMR. *The Log Analyst* 38, no. 2: 84–94.

Walsh, D., P. Turner, E. Grunewald, H. Zhang, J.J. Butler, E. Reboulet, S. Knobbe, T. Christy, J.W. Lane, C.D. Johnson, T. Munday, and A. Fitzpatrick. 2013. A small-diameter NMR logging tool for groundwater investigations. *Groundwater* 51, no. 6: 914–926. https://doi.org/10.1111/gwat.12024

Xiao, L., and K. Li. 2011. Characteristics of the nuclear magnetic resonance logging response in fracture oil and gas reservoirs. *New Journal of Physics* 13, no. 4: 1–12. https://doi.org/101088/1367-2630/13/4/045003

Zlotnik, V.A., and V.L. McGuire. 1998. Multi-level slug tests in highly permeable formations: 1. Modification of the Springer-Gelhar (SG) model. *Journal of Hydrology* 204: 271–282.

Zlotnik, V.A., B.R. Zurbuchen, and T. Ptak. 2001. The steady-state dipole-flow test for characterization of hydraulic conductivity statistics in a highly permeable aquifer: Horkheimer Insel site, Germany. *Groundwater* 39, no. 4: 504–516.